SDC-92-344

SDC
SOLENOIDAL DETECTOR NOTES

PARTICLE IDENTIFICATION IN SDC: SHOWER MAXIMUM AND PRESHOWER DETECTORS

October 13, 1992

M. Hulbert, I. Leedom, S. Reucroft, D. Ruuska and T. Yasuda
Northeastern University

A. Bhatti, A. Maghakian, P. Melese, R. Rusack and A. Titov
The Rockefeller University

P. Bonamy, G. Comby, J. Ernwein, J.R. Hubbard and P. LeDu
CEN Saclay

H. Fenker
SSC Laboratory

A. Wang
University of South Carolina

P. Cushman and S. R. Hou
Yale University

PARTICLE IDENTIFICATION IN SDC:
SHOWER MAXIMUM AND PRESHOWER DETECTORS

PRISCILLA CUSHMAN
Yale University, 260 Whitney Ave.
New Haven, Connecticut 06520, USA

Representing the Shower Maximum Subsystem

A. Bhatti[2], P. Bonamy[3], G. Comby[3], P. Cushman[6], J. Ernwein[3], H. Fenker[4], S.R. Hou[6], J.R. Hubbard[3], M. Hulbert[1], P. LeDu[3], I. Leedom[1], A. Maghakian[2], P. Mélèse[2], S. Reucroft[1], R. Rusack[2], D. Ruuska[1], A. Titov[2], A. Wang[5], T. Yasuda[1] [1]

ABSTRACT

Specially instrumented layers of the SDC tile/fiber calorimeter are used to aid in particle identification. A finely segmented double layer at shower maximum locates the particles with a precison of 2.5 mm and is capable of rejecting events with overlapping π^0's or γ's which can fake electrons and distinguishing between single γ's and π^0 with well separated daughter γ's. When the first layer of the calorimeter tower is read out separately, its early sampling improves electron/charged pion separation by a factor of 5-15 even after shower spreading cuts and E/p. It also provides a "massless gap" correction for energy lost in the coil. Extensive Monte Carlo's and a beam test of the prototype calorimeter including shower maximum and preshower detectors establish the performance of this device.

Development of cost-effective fiber readout for the 48,000 channels of shower maximum is proceeding along 3 lines: improved multi-channel PMT's , avalanche photodiode arrays, and PMT's employing the diode arrays as a photoelectron target. Advances in this technology are also discussed.

1. Introduction

Electron and photon identification can be achieved with standard calorimeters by using global properties of the shower, such as total electromagnetic energy deposited, transverse sharing between towers, the ratio of EM energy over tracking momentum, and the ratio of electromagnetic to hadronic energy. Additional electron identification can be provided by sampling the energy and distribution of the electromagnetic shower at a particular depth. Preshower detectors sample the early part of the shower at 1-3 X_o. At this depth, the electromagnetic showers have begun to develop, but the depth in nuclear interaction lengths is so shallow that only a small fraction of the charged pions have interacted. Thus preshower detectors can provide an additional factor in pion rejection over and above that provided by calorimeter cuts. In addition, undetected energy from electron showers which

[1] 1. Northeastern University; 2. The Rockefeller University; 3. CEN Saclay; 4. SSC Laboratory; 5. University of South Carolina; 6. Yale University

initiate inside the SDC coil (which represents 1-2 X_o's of dead material between $\eta=0$ and $\eta=1.3$) will degrade the electromagnetic resolution. The energy deposited in the preshower detector is related to the amount of shower energy lost in the coil and can be used to correct for this degradation in resolution.

Shower maximum detectors are typically located at around 6 X_o. Since charged pions which interact within the calorimeter will generally deposit a significant amount of energy at this depth, e/π cuts at the shower maximum are highly correlated with those formed using the calorimeter and do not provide as significant an additional pion rejection in combination with them as do preshower detectors. Shower maximum detectors have the advantage of sampling the depth at which most of the shower energy is deposited which relaxes demands on photodetection sensitivity. With a segmentation of 8 strips per $\Delta\eta = .05$ and $\Delta\phi = .05$, energy sharing gives position resolutions of 2.5 mm. This aids in track-shower matching and thus in reducing the background of overlap events in which charged pions with accompanying γ's or π^0's resemble electrons.

Segmentation also means that π^0's decaying to 2 well-separated γ's can be distinguished from single γ's on an event by event basis in the Shower maximum detector. At π^0 energies above 100 GeV, however, this method becomes increasing inefficient due to the small $\gamma-\gamma$ opening angle. A complementary method is offered by the preshower detector which can distinguish between π^0's and γ's statistically, based on the conversion probabilities of one vs two photons. The conversion method is not dependent on the incident particle's energy

2. Baseline SDC Shower Maximum and Preshower Design

The design of the SDC tile/fiber electromagnetic calorimeter (EMC) consists of $\eta \times \phi = .05 \times .05$ towers of alternating 4 mm lead and 4 mm scintillating tiles. The scintillator is read out by 1 mm diameter wavelength-shifting fibers which are spliced to clear optical fibers. The light from the tiles in each tower is optically summed by bundling the clear fibers together at the face of a phototube.

Two special purpose layers are envisioned for the calorimeter. The first layer of tiles can be used as a scintillator analogue of the "Massless Gap" layer in some liquid argon calorimeters. Such a preshower detector (PS) forms the first layer surrounding the solenoid, and is thus sensitive to shower fluctuations which deposit energy in the dead material of the coil. Such a layer would consist of a thicker scintillating tile than the normal EMC tile and would be read out separately from the rest of the EMC tower.

A second special region at 6 X_0 is reserved for the shower maximum detector (SM). These two tile layers would consist of 8 ϕ strips and 8 η strips, each strip being read out by a wavelength-shifting fiber down the center of the strip. The wavelength-shifter is spliced to a clear fiber which must be routed through the cracks between towers to the back of the electromagnetic calorimeter, where each fiber will be coupled to independent channels on a multichannel phototube or avalanche photodiode array. This detector measures the transverse electromagnetic energy profile in the region of maximum energy deposition.

3. Prototype Detectors and Beam Test

An SDC calorimetry test beam run, experiment T841, was conducted at Fermilab during the Summer and Fall of 1991. The purpose of the test was to study the performance of the individual components, as well as their correlation with each other, in a configuration resembling the SDC calorimeter in the barrel region.

The data were collected in the MP9 beam line with incident particle momenta determined to 3.5% (1.55%) for 10 GeV (100 GeV) particles. There were twelve planes of 2 mm pitch proportional wire chambers at three stations for tracking, and two threshold helium Čerenkov counters for electron identification. Muon's were identified by a coincidence between a pair of scintillator counters forming a sandwich with three feet of steel and located behind the hadron calorimeter. Approximately 3-9 % of the events that fire neither Čerenkov are tagged as muons.

The trigger required the beam particles to pass through a 1 cm square finger counter which was centered on one EMC tower. In the data sets requiring only electrons, a coincidence of both Čerenkov counters was required and no muon tag. The charged pion events required both Čerenkov's to have no signal and no muon tag. The Čerenkov efficiencies for detecting electrons changed with beam momentum from 88% and 97% at 15 GeV to 42% and 36% at 50 GeV. For the π^-/e^- rejection results, it was necessary to correct for the Čerenkov efficiencies. The data presented in this paper came from beam tunes that produced electrons and pions with momenta between 15 and 100 GeV.

The SDC Calorimeter test beam contained the following elements (starting from upstream):

1. A simulated SDC coil consisting of 9.2 cm of Aluminum (1.03 X_0) in the following configuration: 0.7 cm Al, 11.3 cm air, 7.5 cm Al, 14.5 cm air, and 1 cm Al.

2. A scintillating fiber PS, consisting of two superlayers, separated by 1 X_0 of lead. Each superlayer was made up of three 1 mm fiber ribbons aligned horizontally and at $\pm 15°$ with respect to horizontal. The fiber ribbons were made with two staggered layers, where each layer contained one hundred 1.0 mm diameter scintillating fibers at a pitch of 1.33 mm. The light from one end of each of the 1200 fibers was detected individually by an image-intensifier/CCD system, and read out using a custom Fastbus digitizing board[1]. The other end of the fibers were read out either with multi-channel photomultipliers or avalanche photodiodes to test these alternative readout techniques. See Fig 1 for detail

3. The tile/fiber EMC consisting of twenty lead samplings of 1 X_0 with 4 thick scintillator tiles. The tiles from each 10 $\times$10 cm^2 tower were read

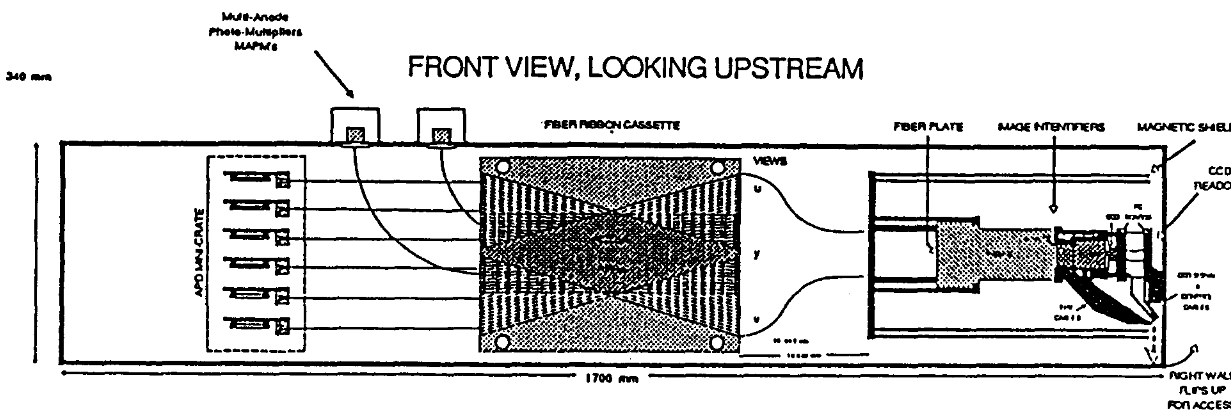

Figure 1: The Position Sensitive Preshower Detector

by WLS fibers, spliced to clear fibers. The clear fibers for each tower were bundled to a single phototube.

4. The strip/fiber SM, containing 12.75 mm wide, 2.5 mm thick individually isolated scintillating strips. There were eight SM strips in each EMC tower at a depth of 6 X_0. The strips were individually read out by WLS fibers, coupled by an optical connector to clear fibers which carried the light to a multi-channel photomultiplier. See Fig 2 for details.

5. The tile/fiber hadronic calorimeter (HAD), constructed from 1 inch thick iron plates and 2.5 mm thick scintillator tiles. Like the EMC, the tiles from each tower are read out by WLS fibers and spliced to clear fiber which are bundled to a single phototube.

3.1. Performance of Preshower Detector

The performance of the position sensitive PS provided detailed information on the average electron shower profile and the track to shower matching at various depths inside the calorimeter. It was compared with the data from the less finely segmented SM detector at 6 X_0. When placed at a depth of 1-2 X_0 it could be used to simulate the response of a non-segmented tile PS. In this case the total energy deposited in all 6 layers of each superlayer was summed. The first superlayer (PS1) was placed after the 1 X_0 of aluminum representing the coil and the second superlayer (PS2) was located 1 X_0 of lead deeper in the shower. These PS samplings were used in the EMC resolution correction and the combined π^-/e^- rejection results presented below.

The PS was used to determine the average shower profile for 35 GeV electrons at depths of 3 and 7 X_0 of lead (without the aluminum coil simulator). The average shower profiles displayed in figs 3a and b, for 3 and 7 X_0 respectively, were produced by superimposing individual showers, normalized by the total shower energy, so that

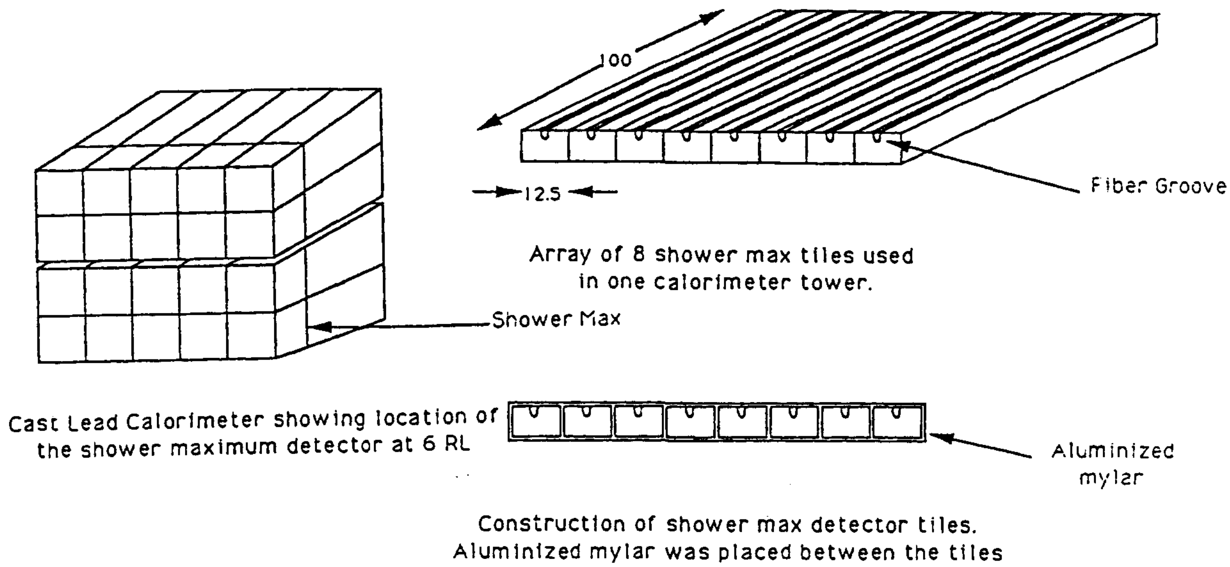

Figure 2: Prototype Shower Maximum Detector used in Beam Test

their centroids were aligned at 0.0 mm on the horizontal axis. The plots display the distribution of fiber pulse height about the shower centroid in millimeters. Since the distributions are clearly non-Gaussian, the widths are characterized by the full width at half maximum which is 9 mm at 3 X_0 and 17 mm at 7 X_0.

The resolution for track-shower matching in the segmented PS was limited by the accuracy of the proportional wire chamber track which was 1.2 mm in this view. Subtracting that inherent resolution in quadrature from the σ of a Gaussian fitted to the track-shower residuals gave resolutions of 1.33 mm (0.67mm) for 35 GeV (50 GeV) electrons at 7 X_o.

3.2. Performance of Prototype Shower Maximum Detector

The shower shape as measured by the SM is shown in fig 4. Also plotted is the shower shape as determined by the finely segmented PS when located at the same depth as the SM and rebinned with the segmentation of the SM. The 2 shapes match only when a 5% crosstalk between neighboring strips is simulated in the PS data. This is consistent with the optical crosstalk expected across neighboring pixels on the multi-channel phototube used to read out the SM. The track-shower residuals were fitted to a Gaussian and a resolution of 2.50 mm was obtained. In the view where this measurement was made the tracking chambers had an inherent resolution 0.5 mm, this was subtracted in quadrature.

The bulk of the data collected had a resolution of σ_E/E=42% at 35 GeV. Shortly before the end our data collection the optical coupling between the SM and the photodetector was remade and the MCPMT was replaced, this improved the resolution to σ_E/E=20%, consistant with our expectations based on Monte Carlo

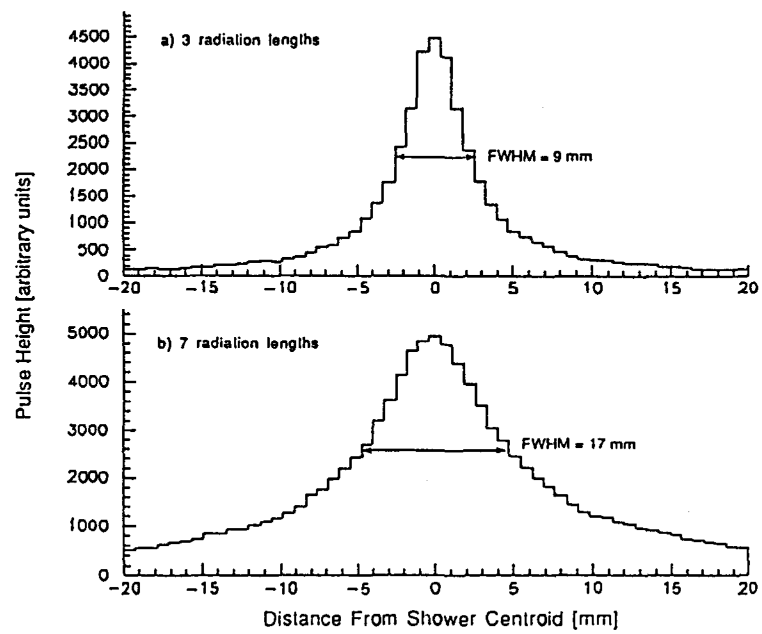

Figure 3: 35 GeV Electron Shower Profile at 3 and 7 X_0

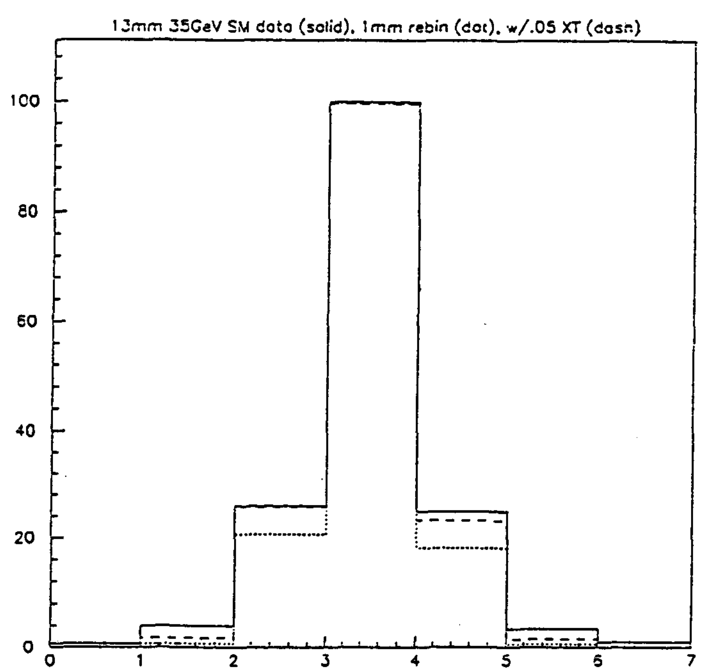

Figure 4: 35 GeV electron shower shape measured in the SM (solid) and in the fiber PS when located at shower maximum and rebinned to correspond to the SM (dotted). Dashed line includes 5% crosstalk.

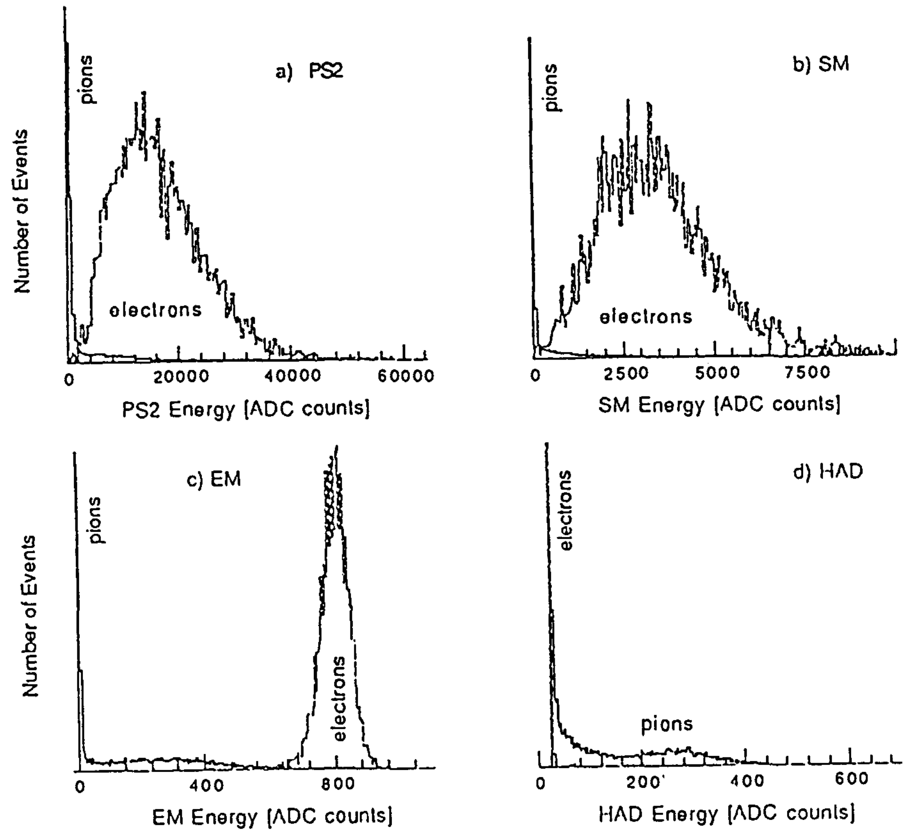

Figure 5: Distributions of Energy Deposited by Pions and Electrons at 35 GeV in the Various Elements of the SDC Test Calorimeter

simulations.

4. Electron Identification

The efficiency for identifying electrons and charged pions was computed for each of the four detector elements in the test beam calorimeter configuration independently and in combination with each other. The coil simulation (1 X_0 Al) and the PS (1 X_0 Pb) are in front of the EMC, so the SM sees a total of 8 X_0 of material in front. The energy deposited in the PS2 (a), SM (b), EMC (c), and HAD (d) for both charged pions (solid line) and electrons (dotted line) at 35 GeV are shown in fig 5.

Threshold cuts on each of the four detector elements were used to determine how well each element could reject pions on their own, producing fig 6 for 35 GeV electrons. Each point on this figure represents the percentage of pions surviving a pulse height cut on one of the detectors versus electron acceptance.

We then compared the charged pion rejection power of the PS and SM detectors for pions that already satisfied both an EMC E/p cut and an electron iden-

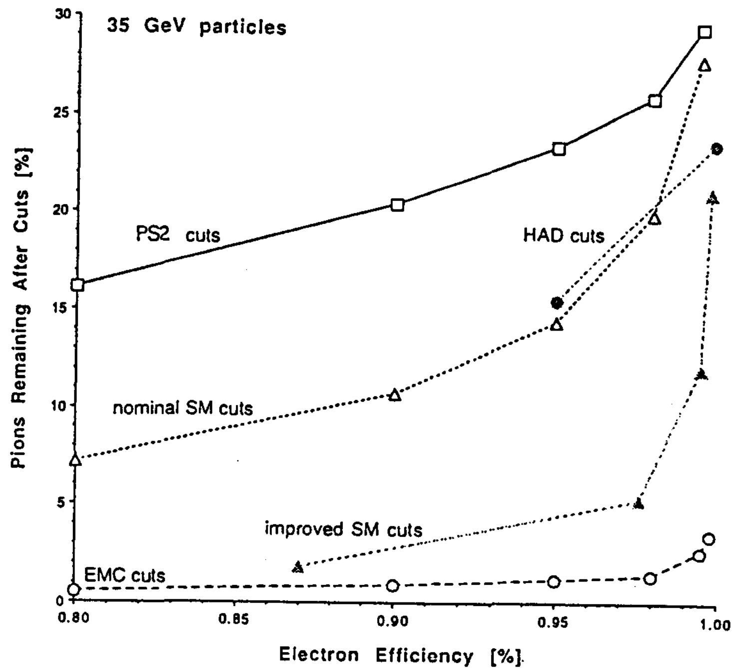

Figure 6: Pions remaining after Individual Cuts on PS,SM, EMC, and HAD Versus Electron Acceptance

tification using the HAD. Fig 7 shows the relative performance, after EMC and HAD cuts, of the PS2 compared to the SM for 15, 35, and 50 GeV. The error bars correspond to the statistical and systematic errors added in quadrature. Here it becomes clear that although the SM has more pion rejection power on its own, the additional rejection possible in conjunction with calorimeter cuts is not as powerful as that due to the PS2. For example, at 15 GeV for 95% electron acceptance 3% of the pions remain after the PS2 cut, while 6% of the pions remain after the SM cut.

For the data set at 35 GeV in which the SM readout was improved, the charged pion rejection was better. The improved data set is also plotted in fig 6. After cuts on EMC/p and HAD, the additional pion rejection provided by PS2 is still more efficient than the improved SM. Although not shown on the figure, when the PS2 and SM cuts are used together, the SM cut does not significantly improve the e/π rejection.

5. Corrections to the EMC Energy Resolution

The barrel SDC electromagnetic calorimeter will be situated behind the magnet coil, which corresponds to 1 X_0 of material at $\eta=0$, and 2 X_0 at $\eta=1.3$. Fig 8 shows the EMC resolution σ_E/E [%] versus the electron beam momentum for varying thicknesses of material in front of the calorimeter: no material, 1 X_0 (Aluminum), and 2 X_0 (Aluminum + Lead). The EMC resolution for the no material case does not represent the optimal EMC resolution achievable. Corrections for beam momentum tagging, tower to tower gain variations and pedestal variations were not

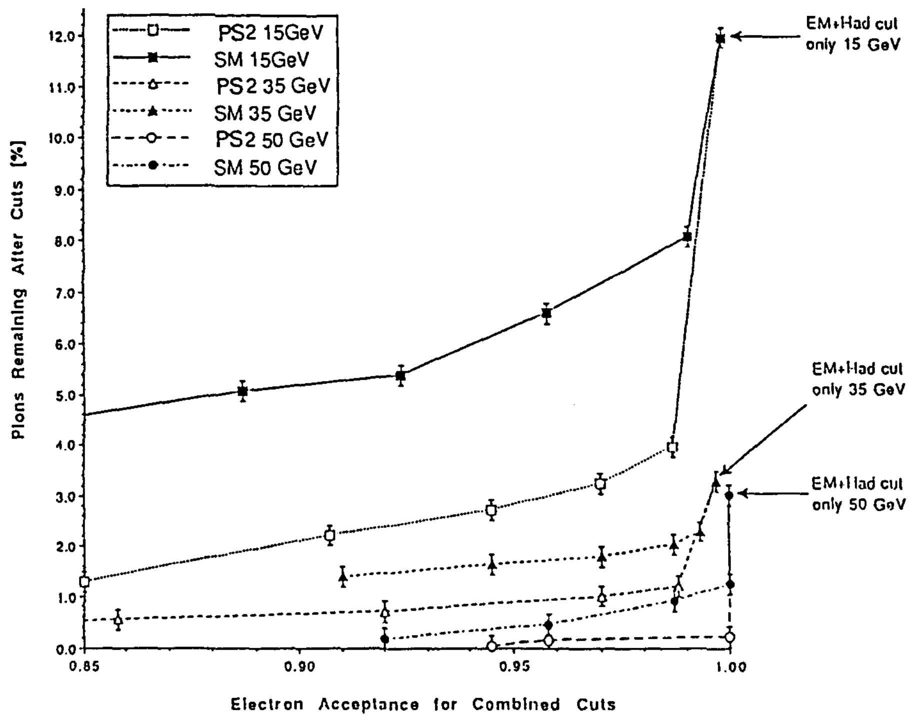

Figure 7: Pions remaining versus electron acceptance for PS2 and SM cuts made in conjunction with EMC and HAD cuts.

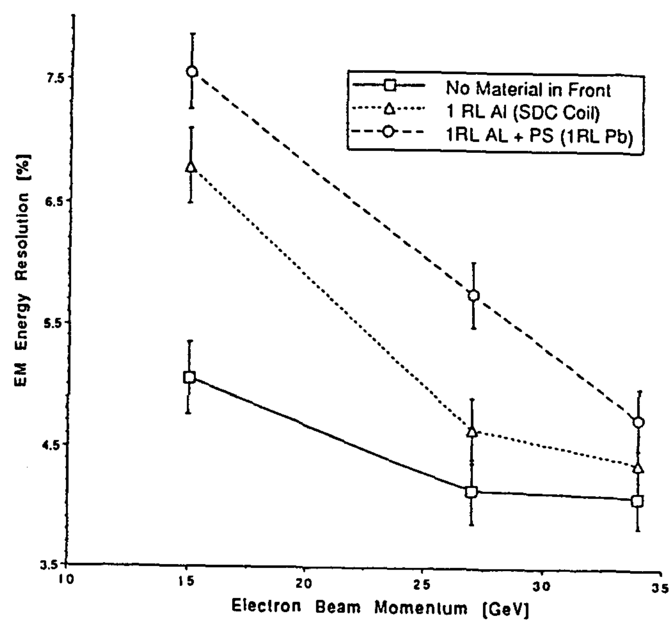

Figure 8: EMC Resolution versus Beam Momentum for various amounts of material in front of the calorimeter.

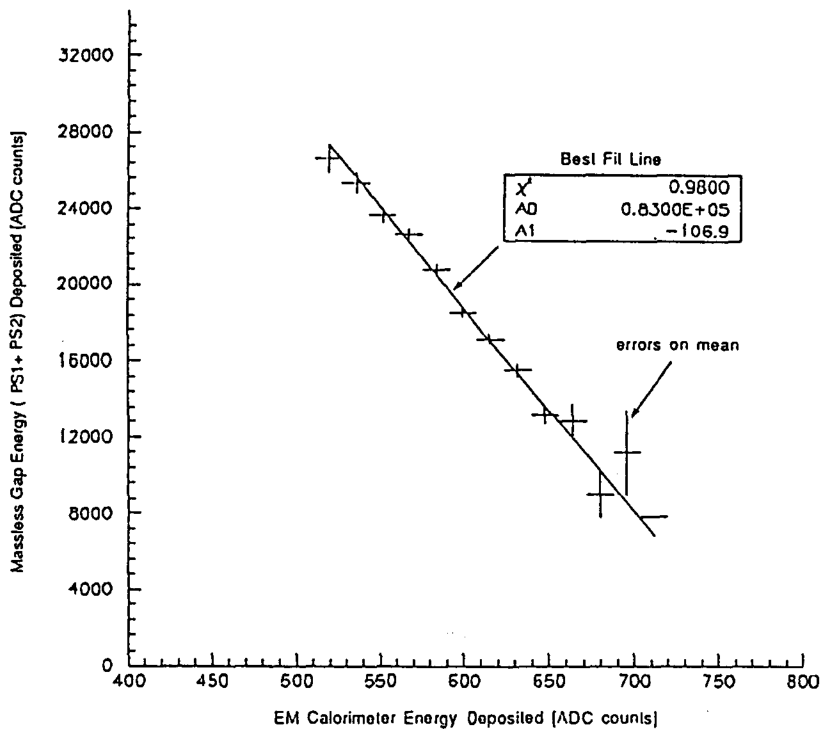

Figure 9: Energy deposited in the PS versus that deposited in the EMC for 27 GeV electrons.

optimized and therefore this should be treated as a comparative study only. The energy lost in the coil is correlated with the detected energy in the PS and therefore anti-correlated with the mean energy measured in the EMC. Fig 9 illustrates this point. The error bars represent the error on the mean and the ratio PS2/EMC can be fit to a straight line with slope -106.9.

The PS energy must be added to the EMC energy with an appropriate weighting factor W, where $E_{corrected} = E_{EM} + W * E_{PS}$. A weight of 0.0 represents no PS2 correction and 1.0 represents the slope of the data in fig 9. In fig 10, the resulting EMC resolution $\sigma_E(\%)/E$ versus the weighting factor W for the PS2 energy shows a clear minimum. The error bars represent the systematic variation of the resolution with different fitting procedures. The optimal weighting factor for both 15 and 35 GeV data is around 0.2 for the PS2 correction. Using this method we obtained the resolution improvement versus beam momentum shown in fig 11 for 2 X_0 of material in front of the calorimeter. The PS1 correction is less effective since it is using energy deposited at 1 X_o to correct for 2 X_o of dead material.

6. π^0/γ Separation

Associated production of the Higgs ($p\bar{p} \rightarrow H + t\bar{t}$) where $t \rightarrow Wb$ and $H \rightarrow \gamma\gamma$ may be the best way for the SDC to identify the intermediate mass Higgs. Since misidentified π^0's form an important background in recognizing the relatively

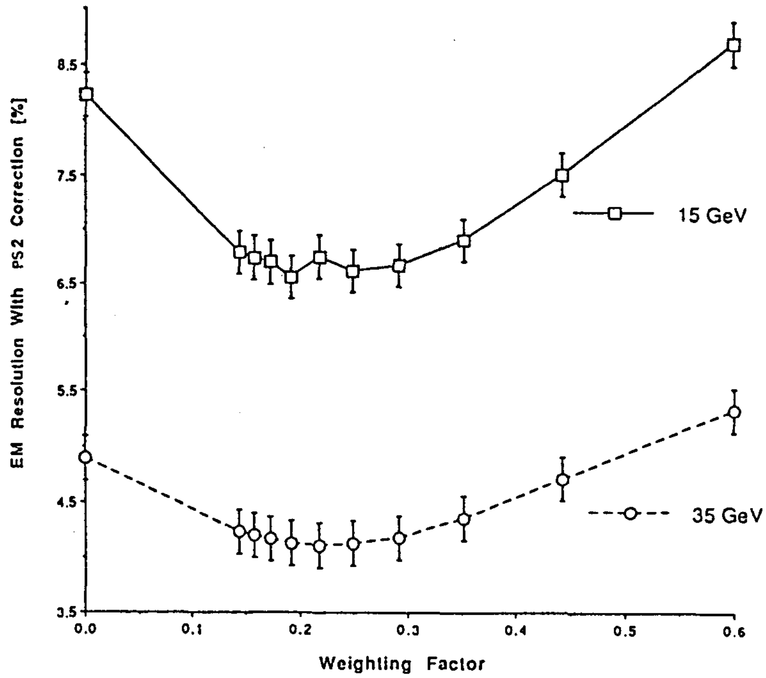

Figure 10: EMC energy resolution versus PS2 weighting factor.

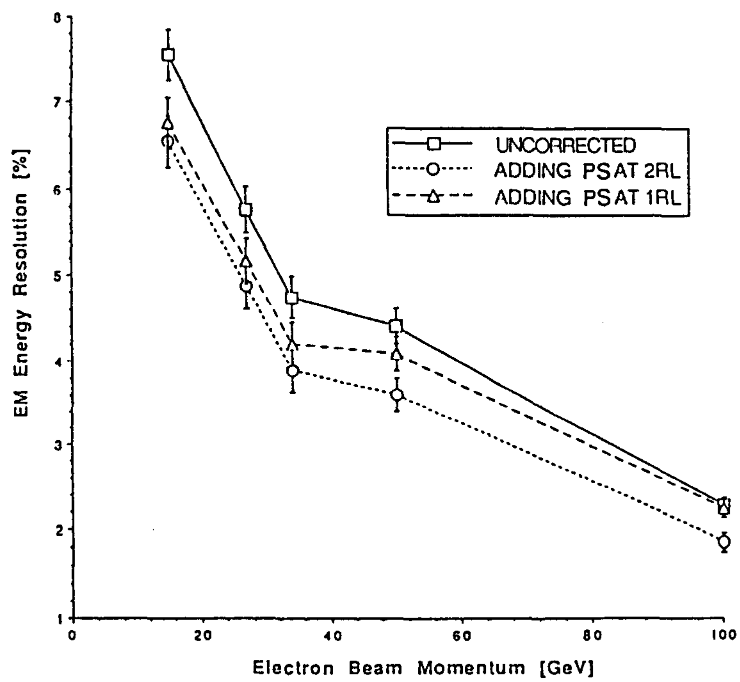

Figure 11: EMC energy resolution versus beam momentum with and without the PS1 and PS2 corrections

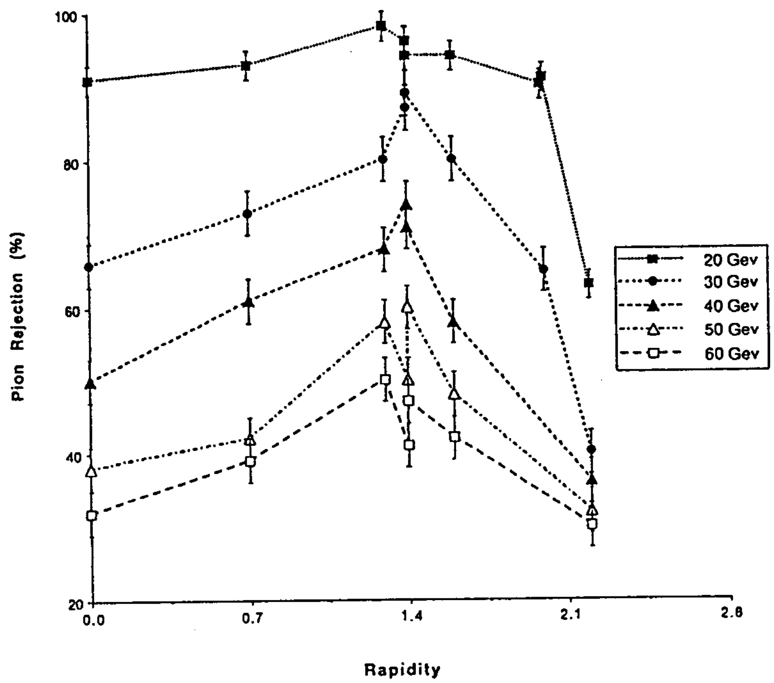

Figure 12: The efficiency for rejecting $p0$'s when χ^2 cuts produce 80% γ identification efficiency in the SM detector. Plotted as a function of η for a barrel and endcap SDC geometry.

isolated photons, Monte Carlo studies were performed in order to determine how well the SM could perform in distinguishing π^0's from single γ's. In these studies only the efficiencies for separating γ's from two close by photons from π^0 decay were studied. The photons from the π^0 decay were required to impact the SM within a fiducial volume of 20×20 cm^2. Inefficiencies due to conversions in the tracking volume or decays of the π^0 where the photons are outside of the fiducial volume were not included in these studies.

Five different Monte Carlo generated gamma profiles were compiled, corresponding to 5 different incident positions within a single strip. These model profiles were then compared to γ's and π^0's with the same calculated centroid, and χ^2 distributions were generated for the two species. This was actually done separately in the 2 orthogonal views and the maximum χ^2 was chosen for the distribution since the $\pi^0 \rightarrow \gamma\gamma$ can be well separated in one view, but not in the other. By choosing a χ^2 cut which gives an 80% detection efficiency for γ's, the efficiency for rejecting π^0's goes from $\sim$ 95% at 20 GeV down to $\sim$ 40% at 60 GeV in the barrel region. A 20% π^0 efficiency would constitute full mixing of γ and π^0 events. There are variations as a function of η, including the crack between barrel and endcap. The results are presented in fig 12. For twice as many shower maximum strips per tower (i.e. 16 strips per tower $\sim$ 6mm strip width), the results are improved: the average π^0 rejection efficiency runs from 100% at 20 GeV down to 60% at 60 GeV, but such fine segmentation is probably ruled out in the barrel by mechanical and budgetary considerations.

Preshower information can also be used to distinguish γ's from π°'s on a statistical basis. For example, the particles impacting the coil at $\eta=0$ will see 7/9 of a photon interaction length, so that $e^{-7/9}$ or 46% of the photons will not interact, and therefore deposit no energy in the PS immediately following the coil. The π°'s however will be seen as two γ's, for which the probability of both γ's not interacting is 21%. To purify a γ sample, we could require that there is no signal in the PS, which would accept 46% of the γ's and provide a signal to background (γ/π°) acceptance ratio of .46/.21 = 2.2. At η=1.3 the γ/π° acceptance ratio is 4.7, but the γ acceptance is only 21%.

7. Research and Development on Fiber Readout

The development of the fiber readout for the Shower Maximum detector poses significant technological challenges. The photodetector must meet the following set of specifications:

1. A linear dynamic range of 4000 to cover 10 GeV to 500 GeV showers, including fluctuations and sensitivity to energy deposited in neighboring strips for shower centroid measurements,
2. Sensitive to a minimum of 10 photons,
3. Crosstalk between neighboring channels of <1%,
4. Channel-to-channel variations of <3:1 across the face of the device,
5. High bandwidth to enable event separation between SSC bunches, and
6. All this at a cost of <$40./channel.

There are three different types of technology under consideration: multichannel photomultiplier tubes (MCPMT), arrays of avalanche photodiodes (APD), and proximity focussed image tubes with an array of APD's serving as the anode (APDPMT). The MCPMT is a conventional device currently available from industry at a cost of approximately $50./channel. The APD is also an established technology, but recent advances in manufacturing and packaging have resulted in devices whose performance is better suited to our application. The APDPMT is a novel technology developed by groups at Rockefeller and Yale in collaboration with industry. It overcomes the principal difficulty of using APD's, poor signal to noise at low photon levels, by converting the incident photons at a photocathode to photoelectrons and accelerating them to several keV before they impact on the APD. There one electron-hole pair is formed for every 3.6 eV of electron energy.

7.1. Multi-channel PMT's

MCPMT's are now made by both Hamamatsu and Philips in 64, 96 and 256 channel versions. These are independent channel devices with low crosstalk between pixels, not to be confused with crossed-wire position sensitive tubes or the

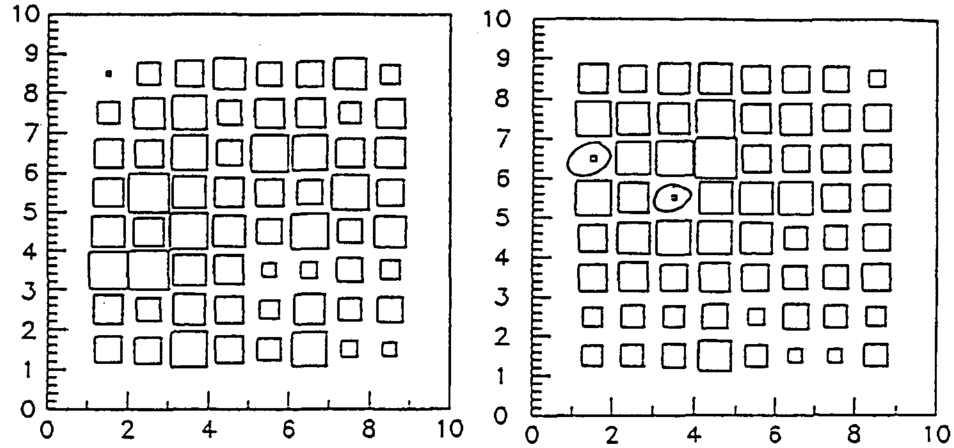

Figure 13: Map of the gain uniformity of 2 different Philips XP4722 tubes. The gain is proportional to the linear dimension of each box, not the area. The 2 channels circled have low gain due to the electronics, not the tube itself.

earlier 60% crosstalk 4140 MCPMT made by Hamamatsu. The Philips XP1720 series achieves amplification through 10 stages of perforated foils and the signals are delivered from a segmented dynode[2]. The Hamamatsu 4140-mod01 is a more conventional mesh dynode design with physical separators to reduce crosstalk (the mod01 part) and a segmented anode. The segmented output for both tubes is at a 2.54 mm pitch. We have characterized these tubes in the lab as illustrated by figures 13-16. Although shown for the Philips tube, the Hamamatsu has similar characteristics.

Although they represent a presently available alternative, they do not meet all the specifications listed above. In particular, crosstalk for realistic fibers arrays coupled to the fiber optic faceplate of the tube is between 2-5 % and the channel-to-channel uniformity averages 4:1 with some channels down by a factor of 10. Conventional green-enhanced photocathodes have quantum efficiencies of 10-12 % in the spectral region (520 nm) of the wavelength-shifting fibers which means that our minimum signal corresponds to only 1-2 photoelectrons. The tubes saturate near 100 pCoulombs for 25 ns wide pulses (see Fig 16), which means that the dynamic range (defined as range from minimum detectable signal to saturation) depends on the gain of the tube. To obtain the required dynamic range of 1000, the gain has to be set such that the minimum signal, corresponding to one photoelectron, is 0.1 pC. Finally, the cost of the Philips 64 channel XP1722 is ~ $5000 (comparable Hamamatsu tubes are 50% more) which brings the per channel cost to >$50.

Some of these issues are being addressed by the respective companies in development projects initiated by the Shower Maximum Collaboration. Philips is rearranging the pixel design and improving the photocathode deposition process to produce a green-sensitive, 1% crosstalk 68-channel device by January 1993. On the same timescale, Hamamtsu are improving crosstalk by increasing the size of their

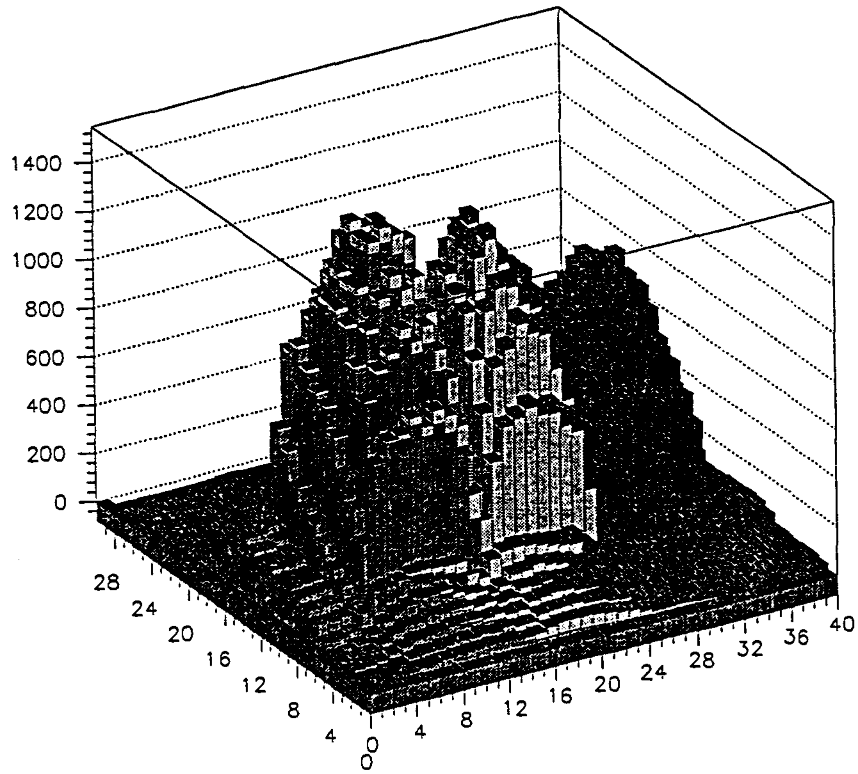

Figure 14: A 500 micron fiber is scanned in one dimension across 3 pixels in .01 inch steps. The response plots of the 3 dynodes are summed.

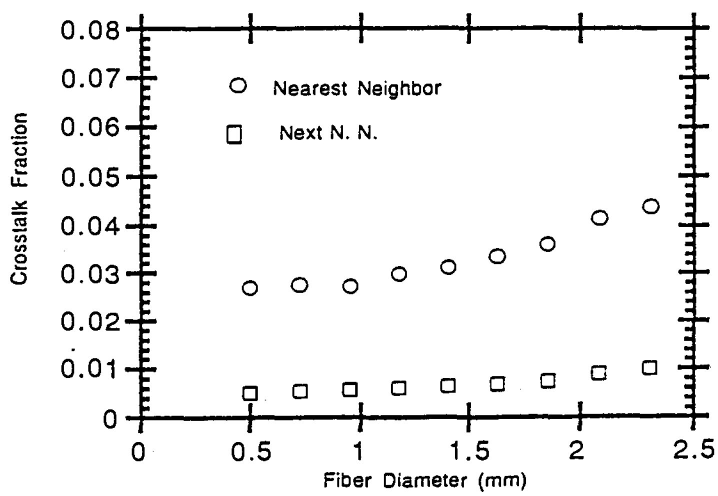

Figure 15: Crosstalk is measured as a function of the fiber diameter using careful centering of the fiber. The crosstalk averaged over all neighbors always increases for off-center fiber placement.

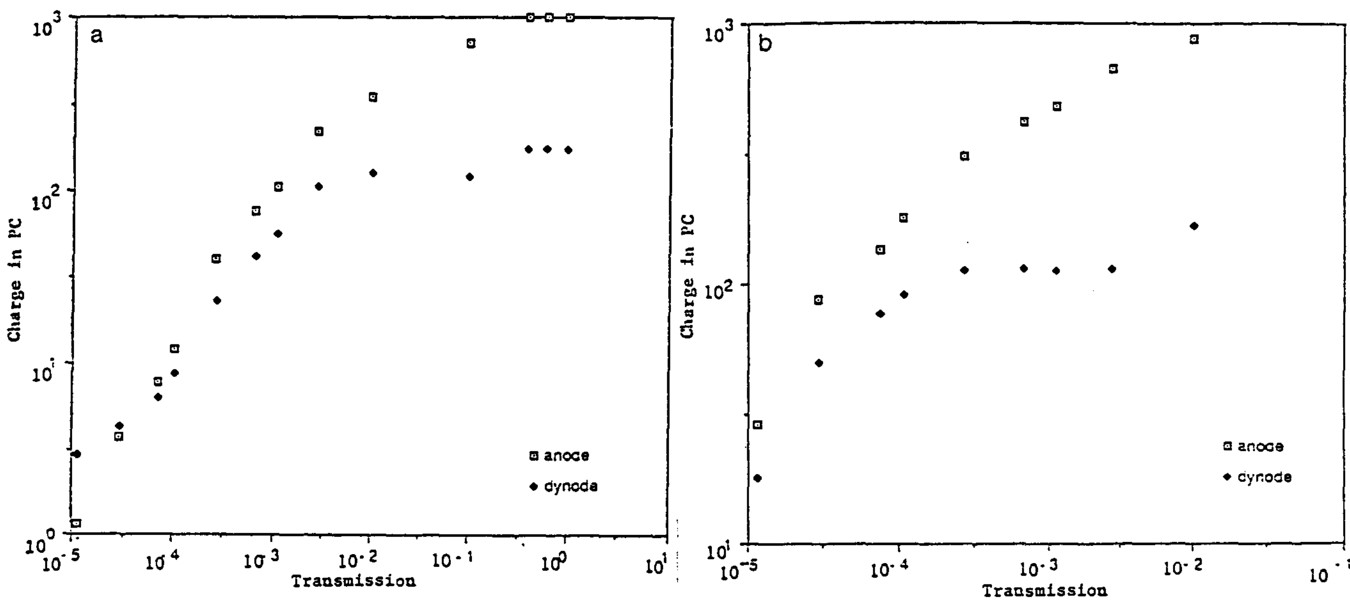

Figure 16: Linearity of dynode and summed anode of the Philips XP4722 for operating voltages of (a) 1000 volts and (b) 1400 volts. This is a log-log plot of the relative light intensity in units of the transmission of calibrated neutral density filters versus the number of pCoulombs in a 25 ns FWHM pulse into 50 Ω's as measured by an ADC.

pixels to 5 mm and improving their quantum efficiency in the green.

7.2. Avalanche Photodiode Arrays

APD's have the advantages of high quantum efficiency (60-80% depending on surface treatment), large dynamic range and compact packaging. However, they typically had low gain (< 100 in the linear region) which was, in addition, sensitive to small fluctuations in temperature and bias voltage, thus limiting their application to light levels of 100 photons or more[3].

Advanced Photonix Inc. has successfully subdivided their 16mm diameter APD's into an array by cutting smooth grooves into the n-side of their wafer. These are large area APD's with a "bevelled edge" design. The breakdown voltage is very high ($\sim$ 2000 volts) with a wide depletion zone. Thus, gains of 250-1000 are achievable while still remaining below breakdown voltage. The k-value, or ratio of hole to electron ionization rates, is only $k = 0.0025$ resulting in a lower excess noise factor and less variation in gain due to nonuniformities in the doping level of the depletion layer.

Adv. Photonix Inc. delivered three 3×3 arrays of 3mm size pixels which form the basis of the test results reported here, and are currently working on an 8×8 array (1mm pixels with 1.27 mm pitch) for the prototype SM readout. The final product will be very cost effective at $580 for 64 channels. The gain curve for the central pixel is shown in fig 17.

There are 2 sources of dark current: a surface current which is independent of gain and a bulk current which is caused by thermally generated electron- hole

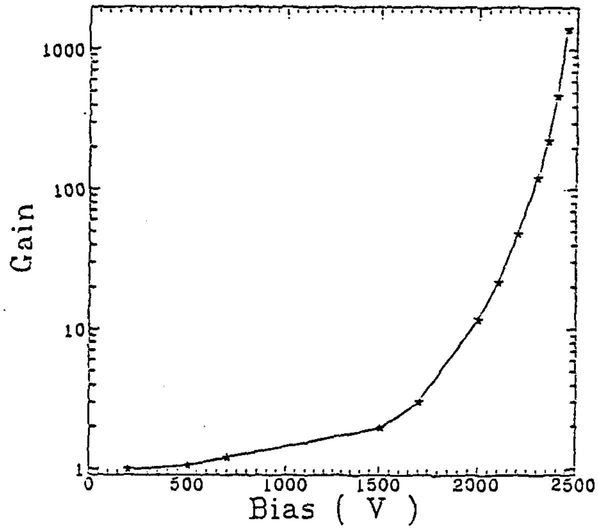

Figure 17: Gain as a function of reverse bias voltage applied to a 3× 3 segmented APD from Adv. Photonix Inc.

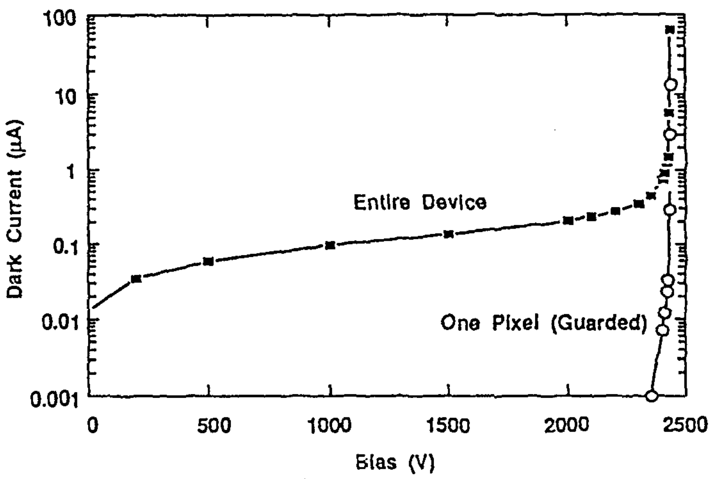

Figure 18: Dark current of the device with and without guard ring. Without guard ring the dark current is dominated by surface current at low gain.

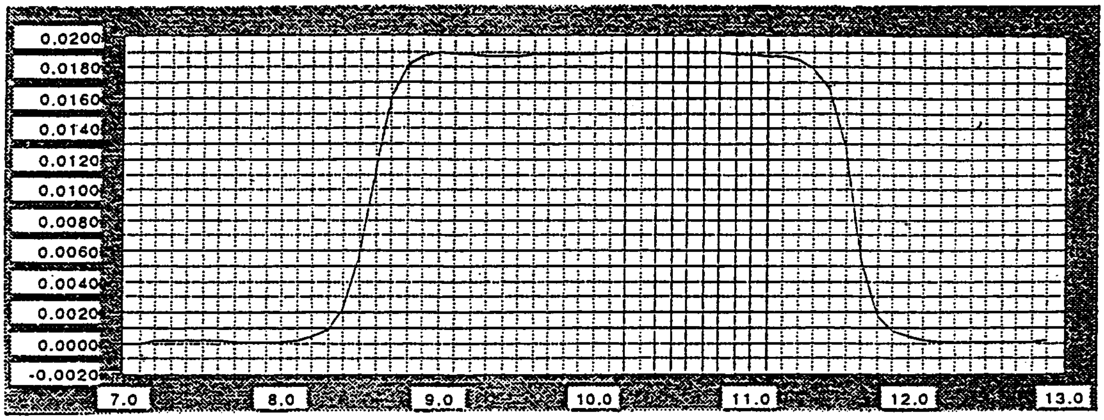

Figure 19: Vertical scan of three 3mm pixels, each separated by a 400 μm groove. The DC light source was a red laser diode with focussed 10 micron spot. Step size was 0.1 mm.

pairs and is thus subject to electron multiplication. The surface current of ~ 100 nAmps can be reduced to picoamperes by sinking it through a grounded guard ring as shown in fig 18. The bulk dark current is proportional to $e^{-a/kT}$ and thus could be reduced by cooling the array. Even at room temperature, however, the bulk dark current is only approximately 2 pAmp/mm^2 or 10 e-h pairs generated every μsec. The minimum signal for the SM is 10 photons, which corresponds to 8 photoelectrons, maintaining a comfortable signal to noise. Of course, since the signal must be electronically amplified, the noise of the amplifier and the capacitance and inductance of all leads must be kept under control. The pixel capacitance is expected to be 4-8 pF. Low noise (200 ENC) amplifiers must be designed to match these specifications which could then be bump-bonded directly to the pixel array.

Crosstalk between pixels was measured in both DC and pulsed mode. In pulsed mode, a fiber directed light from a laser diode onto the center pixel and signals from all 9 pixels were amplified and recorded by an ADC. No crosstalk was observed down to the 2% level which was the best sensitivity possible with this test. That is because for large bias voltages, a pulse of the opposite polarity is induced on the capacitively coupled neighbors at the level of a couple percent. DC crosstalk measurements were done with a laser diode at constant current. A 10 micron spot was focussed on the surface of the APD and scanned in 0.1 mm steps across 3 pixels vertically. The resulting scan is shown in fig 19 and illustrates that the crosstalk is below 0.5%. Crosstalk is a function of the bias voltage and only reaches this level when the depletion zone approaches the tops of the grooves.

7.3. Avalanche Photodiodes in a Phototube

The segmented APD described above can be used to form the anode of a proximity focussed phototube. We plan to do this using the new 8 × 8 array from Adv. Photonics Inc. Several single channel versions using a single 16 mm diameter APD, located 6.8 mm from the photocathode were manufactured last year and all data presented in this paper are from tests of these devices in our lab. The photocathode is maintained at a negative high voltage (8-12 kV), the front surface of the APD is held to ground through a 1 kΩ resistor, and the back surface or anode of the APD is biased with a positive voltage of 1-2 kV. Charge is supplied to the APD anode from a 10 nF storage capacitor to ground and the signal is picked off the APD cathode. No divider chain is required.

The dark currents measured on the set of 8 APD's delivered to Litton for potting ranged from 160-350 nA for 16 mm diameter devices at room temperature. After potting, the prototypes had dark currents of 370 nA and 700 nA, representing a factor of 2 increase after bake-out over the bare APD dark current.

A large area also implies large capacitance; 120 pF is typical for the APD, which results in a large RC constant and thus slow risetime. The 8 APD's had measured risetimes of 15-40 ns. However, for the application in mind: fiber readout of the SDC Shower Maximum Detector, these large area APD's will be subdivided into 8 × 8 arrays, reducing the capacitance such that it no longer influences the risetime.

The APD is operated in electron bombardment mode: photoelectrons are accelerated by the electrostatic field and strike the APD with energies in the keV range. The gain of this first stage is therefore approximated by the photocathode voltage divided by 3.57 eV, once losses at the APD's surface are accounted for. An additional gain of 200-1000 is provided by the APD itself, yielding an overall tube gain of 5×10^5. Because of the first stage gain, the signal to noise of the hybrid tube is greatly improved over that of a bare APD operating in the optical mode. The second stage of amplification is not present in hybrid tubes equipped with a PIN diode target, where gains beyond 5000 are difficult to obtain.

The characteristic gain curves have been measured in both pulsed and DC mode. In pulsed mode a scintillator with a spectral peak at 430 nm was activated by a N_2 ultraviolet laser. These curves as a function of both APD reverse bias and gap voltage are shown in fig 20. The gain is extremely linear with applied gap voltage (V_{pc}) above 1000 V, a threshold which depends on the surface treatment of the APD. The gain as a function of reverse bias voltage has a sharp upturn as it approaches the breakdown voltage. The signal to noise also degrades in this region and optimum performance is found at reverse biases <2000 volts.

Measurements of the linearity of this device over 6 orders of magnitude have been performed in both DC and pulsed mode. In the DC mode, a constant light source illuminated the photocathode and the output current was measured directly using an electrometer. In the pulsed mode, blue light from a scintillator activated by a N_2 laser was directed at a 2 mm spot on the photocathode. A series of calibrated neutral density filters reduced the amount of primary light reaching the tube. At the low light end, the signal was amplified by a high speed preamplifier. At the high light end, the amplifiers were replaced by a series of calibrated attenuators. No departure from linearity was observed over 6 orders of magnitude (see fig 21).

By turning off the laser and covering the tube entrance hole, the single photoelectron peak was observed. At V_{pc}=-8 kV, V_{APD}=2 kV, it is well separated from the noise (see fig 22). The signal corresponds to 0.103 pC/photoelectron with

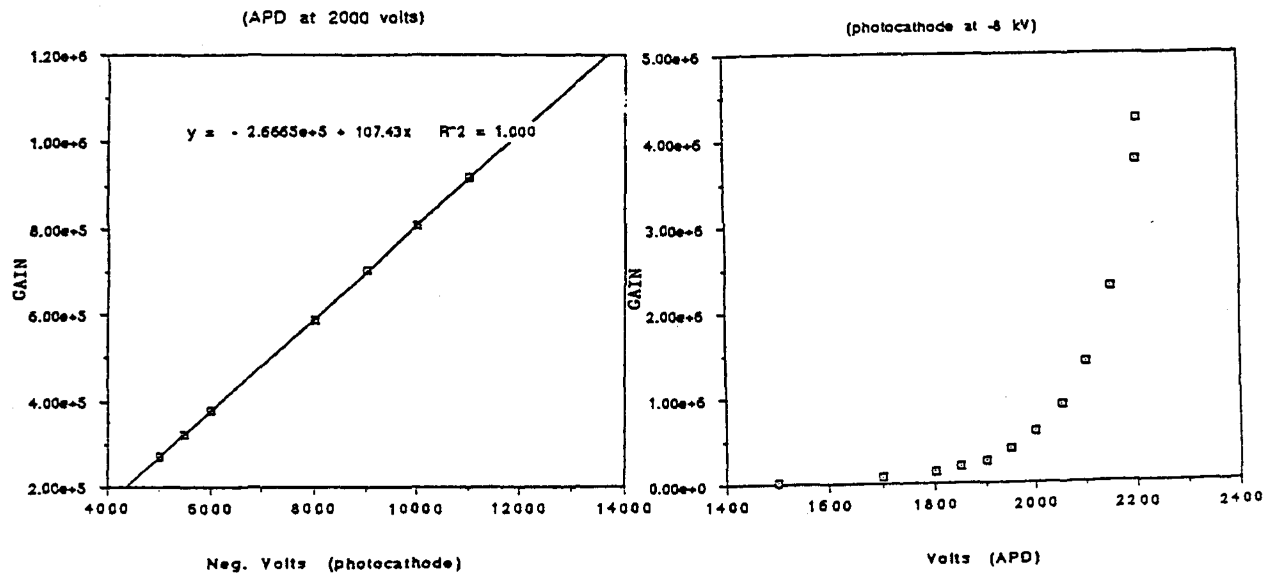

Figure 20: (a) Gain as a function of photocathode voltage for an APD bias voltage of 2 kV.(b) Gain as a function of APD bias voltage for a photocathode voltage of -8 kV.

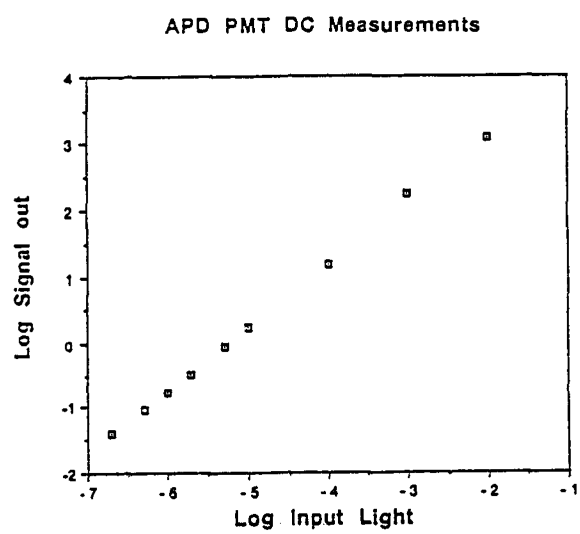

Figure 21: The output charge in picoCoulombs as a function of relative light intensity as defined by the transmission of calibrated neutral density filters.

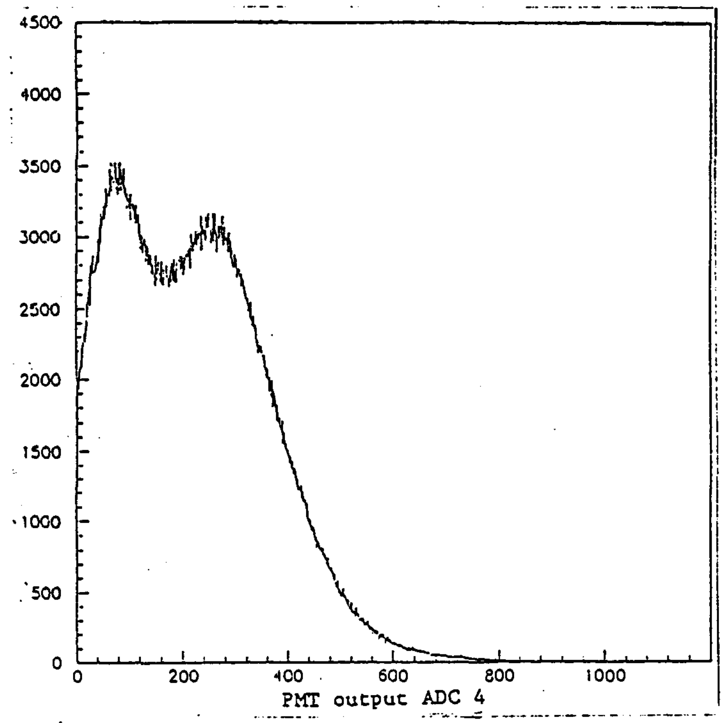

Figure 22: Single Photoelectron Peak and pedestal

σ =48%. At V_{pc}=7 kV, σ is only 33%. A scope trace from the high end of the linearity studies is shown in fig 23. The pulse (no amplification, × 5 attenuation) corresponds to 160 volts into 50 Ω. It shows no evidence of saturation.

An advantage over commercially available MCPMT's is the wide variety of photocathodes that are available through Litton. Tubes with bialkali and S20 photocathodes have been produced. Two tubes with GaAsAl photocathodes were also manufactured, and displayed quantum efficiencies of 34% at 530 nm. It is important to determine the lifetime of these tubes. Electron bombardment could cause damage to the silicon itself, and attendant outgassing can poison the photocathode over time. So far there has been no evidence for damage to the silicon which would result in loss of gain. One of the GaAsAl tubes lost quantum efficiency rapidly and a manufacturing fault is suspected. The second tube has been subjected to a series of tests including the linearity studies which produced instantaneous output currents as high as 5 amps (refer to fig 23). After an integrated running of 0.35 μAmp-hours (1.3 mCoulombs) from the photocathode, the quantum efficiency was measured to be 24%, corresponding to only a 30% reduction.

Nonuniformities in the APD are measured at the 5% level. Since most nonuniformities in conventional phototubes are due to varying collection efficiencies on the multiplying structures, and since the photocathode itself is very uniform, the tube has a less than 10% variation over the active area. This is a very important property for multi-anode versions of the tube, since it means channel-to-channel variations will be negligible, simplifying the requirements on the digitizing

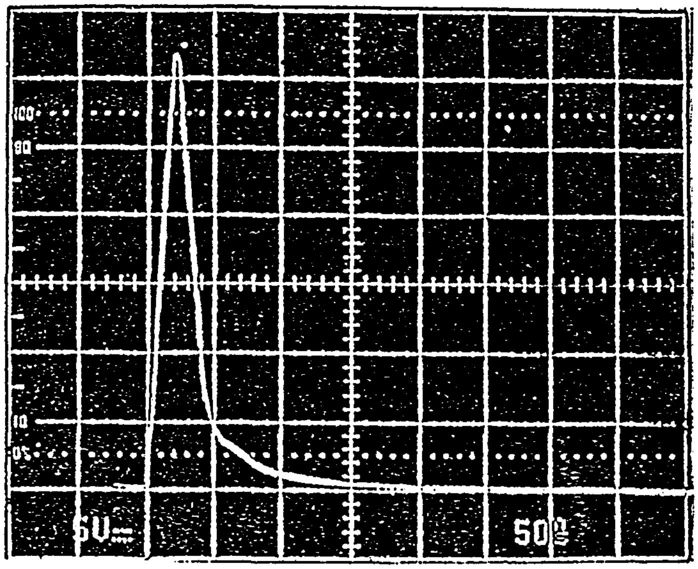

Figure 23: Scope trace of the signal at the high end of the linearity study. The laser is operating without filters and a factor of 5 attenuator is on the scope input. The signal corresponds to 160 volts into 50 Ω, or 3.2 Amps peak output.

and trigger electronics which follow.

We have designed and built a hybrid phototube which exhibits the following features:

1) Gain of 5×10^5
2) Linear over 6 decades
3) Sensitive to single photoelectrons
4) Quantum efficiency of >30%, depending on photocathode choice
5) Resistance to near-axial magnetic fields
6) 10% variation in gain over active area
7) < .1 ns transit time jitter
8) 20 ns risetime limited by area capacitance
9) Simple, low current operation at room temperature

The multi-channel version can be expected to include the following properties:

1) <1% crosstalk based on the measurements of the APD array and the fact that the tube is a simple, small gap planar accelerator.
2) Channel-to channel variations of 1.1:1
3) Only $16./channel
4) <5 ns risetime per channel

8. Conclusions

Particle identification in the SDC detector will be greatly enhanced by the addition of 2 special purpose detectors corresponding to specially instrumented sections of the electromagnetic calorimeter. A simple, non-articulated preshower detector can correct for energy lost in the solenoid, improve the e/π separation, and distinguish between π^0 and γ on a statistical basis. These functions are complementary to those performed by a segmented shower maximum detector which can distinguish between individual π^0's and γ's in the 10-80 GeV range and can improve track-shower matching to identify non-isolated electrons and hadrons with overlapping electromagnetic showers.

The technological problems involved in reading out 48,000 channels of shower maximum information appear to be soluable, although it will require either an extension of current MCPMT and APD designs or the combination of the two into a new hybrid tube. Progress on all three fronts is proceeding rapidly and a decision will be made on the appropriate readout technology by summer of 1993.

9. References

1. P. Melese *et al.*, "Electron Identification and the Detection of Synchrotron Radiation with a Preshower Detector," to be published in NIM.
2. G. Comby and R. Meunier, "Test of a New 64-Channel PMT for Imaging," NIM, Vol A269, p246 (1988).
3. P.P. Webb, R.J. McIntyre, and J. Conradi, "Properties of Avalanche Photodiodes," RCA Review, Vol.35, p234 (1974).